

# HgS NANOPARTICLES FROM CYCLODODECANONETHIOSEMICARBAZONE COMPLEX OF MERCURY AS SINGLE-SOURCE MOLECULAR PRECURSOR

Jisha George<sup>1</sup>, G. Rathika Nath<sup>2</sup>, S. Fasma Das<sup>1</sup>, S. Aswathy<sup>1</sup>, and K. Rajesh<sup>1,✉</sup>

<sup>1</sup>Department of Chemistry, University College (Research Centre, University of Kerala)  
Trivandrum-695034, (Kerala) India

<sup>2</sup>Department of Chemistry, KSM DB College, Sasthamcotta (Research Centre, University of  
Kerala) Kollam-690521, (Kerala) India

✉Corresponding Author: [rajesh\\_k\\_k@yahoo.com](mailto:rajesh_k_k@yahoo.com)

## ABSTRACT

Hg(II) complex of a new ligand cyclododecanonethiosemicarbazone (CDDTSC), was synthesized and characterized by spectral studies and elemental analysis. Synthesis of nano mercuric sulphide was done using the polyol method with glycerol as solvent. UV- Vis spectroscopy, PL, XRD, SEM, EDX, and TEM studies were done for characterization. Though Capping agents or surfactants were not used, highly crystalline, monodispersed HgS nanoparticles were obtained in good yield.

**Keywords:** Mercuric Sulphide Nanoparticles, Single Source Molecular Precursors, Thermal Decomposition, Cyclododecanonethiosemicarbazone.

RASAYAN J. Chem., Vol. 15, No.4, 2022

## INTRODUCTION

Semiconductor HgS nanoparticles have wide applications when compared with bulk materials as a result of size-dependent optoelectric and magnetic properties.<sup>1-3,5,7,9,11</sup> Single Source Molecular Precursor method developed by Brenman and coworkers can be used for preparing superior nanocrystals with a large surface area, minimal flaws, and improved stoichiometry.<sup>4</sup> Single Source Precursor route is recognized as an efficient means to generate semiconductor nanoparticles with uniform metal ion distribution at the molecular level.<sup>6</sup> HgS are important among group II-VI semiconductors for their important optical properties, which are strictly related to the size and shape of these nanoparticles that depend on the quantum confinement. HgS appears in two crystalline forms hexagonal phase ( $\alpha$ -HgS or Cinnabar) with a 2.1 eV band gap and a cubic phase ( $\beta$ -HgS or Metacinnabar) with a band gap of (0.5eV). HgS nanoparticles and thin films have numerous applications in a variety of fields, including ultrasonic transducers, image sensors, photoconductors, electroluminescent diodes, and so on. This paper is focused on the application of the Hg complex of freshly prepared cyclododecanonethiosemicarbazone ligand, as SSMPs in order to create the Hg metal sulphides.

## EXPERIMENTAL

### Materials

The metal salt  $\text{Hg}(\text{OOCCH}_3)_2 \cdot 2\text{H}_2\text{O}$ , Glycerol, Thiosemicarbazide, and cyclododecanone were from Sigma Aldrich, Merck, and TCL respectively.

### Synthesis of Ligand ( $\text{C}_{13}\text{N}_3\text{SH}_{25}$ )

Thiosemicarbazide and cyclododecanone in a 1:1 molar ratio as hot solutions in ethanol were mixed together and refluxed with constant stirring for three hours. On cooling white crystalline precipitate was obtained. Percentage yield 81%. Anal. Cal. for  $\text{L}-(\text{C}_{13}\text{N}_3\text{SH}_{25})$ : C, 61.18; H, 9.8; N, 16.47; S, 12.5. Found: C, 61.14; H, 10.01; N, 16.40; S, 12.3. MS: 256  $[\text{M}+\text{H}]^+$ , 278  $[\text{M}+\text{Na}]^+$ . Significant IR bands: 3405, 3218 ( $\text{NH}_2$  sym and asym), 3142 (N-H), 1593 (C=N), 1076 (N-N), 863 (C=S).  $^1\text{H}$ NMR in ppm

(500MHz, DMSO) : 8.64 (s 1H N-H), 7.24 (d 1H NH<sub>2</sub>), 6.179 (s 1H NH<sub>2</sub>), 2.365-2.340 (t 1H CH<sub>2</sub>), 2.277-2.251 (t 1H CH<sub>2</sub>), 1.709-1.565 (m 2H CH<sub>2</sub>), 1.33-1.25 (t 18H CH<sub>2</sub>).

### Synthesis of Complex

Hg(II) acetate dehydrate solution was added to the ligand in dilute ethanol (water: ethanol = 1:1 by volume), in a 2:1 ratio, with continuous stirring using a glass rod. Grey-colored precipitate was formed. Percentage yield for Hg(II) complex 74%. Anal. Calc. for L<sub>2</sub>Hg - (C<sub>13</sub>N<sub>3</sub>SH<sub>25</sub>)<sub>2</sub>Hg. C, 43.94; N, 11.8; H, 7.04; S, 9.01. Found: C, 43.83; N, 11.74; H, 6.32; S, 8.97. IR (KBr,  $\nu$  = cm<sup>-1</sup>): 3406, 3290 (NH<sub>2</sub>), 3170 (N-H group), 1607 (C=N group), 1089 (N-N group), 832 (C=S group), 554, 512 (M-N group), 460 (M-S group).

### SSMP Metal Complex Preparation

Synthesis of SSMP was done using a method already reported by the authors.<sup>8</sup> The colors of the metal sulphides obtained were black.

## RESULTS AND DISCUSSION

### Characterization of Ligand and Metal Complexes

Elemental analysis and spectral studies were used to characterize the ligand and complexes. Figure-1 shows <sup>1</sup>H NMR and Fig.-2 shows MS(EI) spectra of the synthesized CDDTSC ligand.

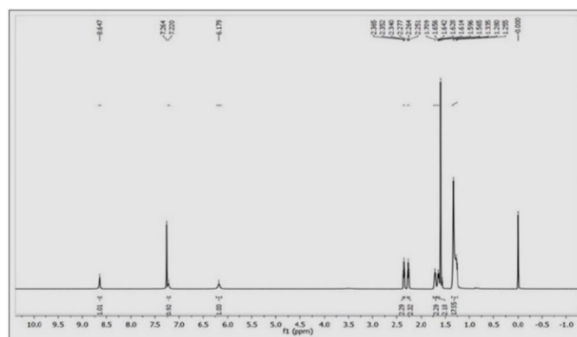


Fig.-1: <sup>1</sup>H NMR Spectrum of CDDTSC Ligand

Broad and medium intensity signals at 3400-3200 and 3180-3141 cm<sup>-1</sup> of IR Spectrum are assigned to the  $\nu_{\text{NH}_2}$  and  $\nu_{\text{NHCS}}$  signals respectively<sup>10,12</sup> and these signals are not much modified by coordination indicating non-coordination of them during complex formation. Non-presence of  $\nu_{\text{SH}}$  absorption at 2570 cm<sup>-1</sup> shows the presence of thione form in the ligand.<sup>17</sup> This is also supported by the 862 cm<sup>-1</sup> (C=S) signal.<sup>13,14</sup> The absorption at 1075 cm<sup>-1</sup> for the ligand is attributed to  $\nu_{\text{N-N}}$ . The frequency increase of this absorption in the spectrum of complexes indicates coordination through azomethine nitrogen.<sup>15,16,18</sup> Absorption at 1592 cm<sup>-1</sup> of (C=N) is shifted to higher frequencies during complex formation. An increase in the (C=N) bond strength which in turn strengthens the N-H in the amide group may be the reason behind this.<sup>19</sup> Coordination of metal ion with sulphur causes displacement of electrons from sulphur, resulting in a decrease in the frequency of vibration of C=S as there will be a weakening of that bond and a reduction in the intensity of this signal for the complex.<sup>20,21</sup> Absorption bands in the 575–500 cm<sup>-1</sup> range relate to Metal to Nitrogen bond vibrations and in the 460-455 cm<sup>-1</sup> range denote M-S bond vibrations.<sup>22</sup> Thus it is clear that CDDTSC is a bidentate ligand and it undergoes coordination with metal atoms through azomethine N and S. The EIMS of CDDTSC (Fig.-2) have a molecular ion peak of greater intensity assignable to [M+Na], [(C<sub>13</sub>N<sub>3</sub>SH<sub>25</sub>+Na)<sup>+</sup>] at 278 amu. There is another peak assignable to [M+H]<sup>+</sup>, [(C<sub>13</sub>N<sub>3</sub>SH<sub>25</sub>+H)<sup>+</sup>] at 256 amu and this confirms the proposed formula. Other important peaks are, one at 239 amu due to the loss of NH<sub>2</sub>, [C<sub>13</sub>N<sub>2</sub>SH<sub>23</sub>]<sup>+</sup> and another at 180 amu due to lose of –NHCSNH<sub>2</sub> group [C<sub>12</sub>NH<sub>23</sub>]<sup>+</sup>. Figure-2 Shows the Thermo Gravimetric Analysis (TGA/DTG) Result of the Hg Complex,

The thermal decomposition profile of the Hg(II) complex shows that the decomposition of the ligand moieties takes place in four stages. The first stage is between 150 – 210 °C. The second stage is between 230 - 340 °C. In this second stage, the inflection point is detected at 283.26 °C, which shows the greatest loss of change in the TG. The third stage at 340- 500 °C, has three consecutive sub-steps of

decomposition. The fourth stage of decomposition starts at 540 °C and the process takes place very slowly leaving only a very small amount of residue. The reason for this is that generally, the mercury complexes are volatile at high temperatures leaving almost no residue.<sup>23</sup>

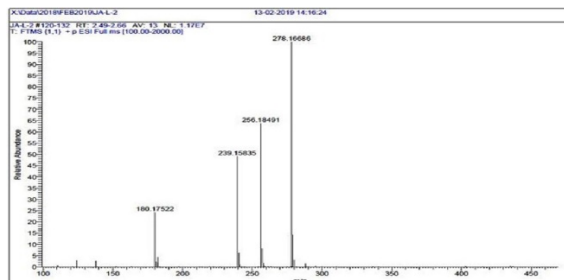


Fig.-2: MS (EI) Spectrum of CDDTSC Ligand

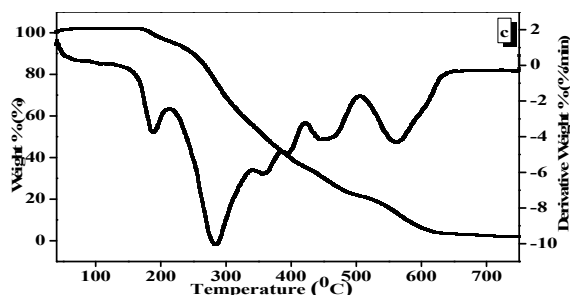


Fig.-3: TGA and DTG Curves for Mercury Complex

### Characterization of the Nanoparticles

Ultra Violet-Visible spectroscopy gives a clear idea about the size distribution of the synthesized nanoparticles.<sup>24</sup> Semiconductor nanocrystallites are widely recognized to have an absorption edge that is switched to shorter wavelengths in comparison to bulk. This shift to higher wave numbers is thus interpreted as evidence of the existence of nanocrystals.<sup>24</sup> When the dimension of a semiconductor crystal is reduced, the band gap widens, and the quantum energy needed to excite electrons to the conduction band is raised, and this results in a shift to higher wave numbers of the absorption edge. Figure-4 shows the UV-Vis spectrum of synthesized Mercuric Sulphide nanoparticles.

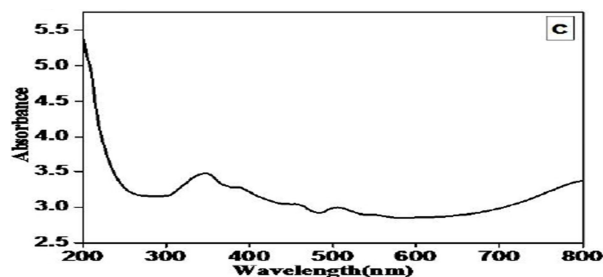


Fig.-4: UV-visible Absorption Spectrum of HgS

Bulk HgS values (563 nm) of the absorption band edge were blue-shifted.<sup>22</sup> It was found that for the prepared HgS the absorption band edge is at 207 nm with shoulders of low intensity at higher wavelengths. This indicates that the HgS nanoparticles may not be strictly monodispersed.<sup>24</sup> In Tauc plot  $[(\alpha h\nu)^2 \text{ vs } h\nu]$  gave band gap ( $E_g$ ) of nanoparticles.<sup>25</sup> Band gap energy of the associated nanoparticles (optical) is measured by extrapolating the plot towards the X-axis. Tauc plots for prepared HgS are shown in Fig.-5.

In the case of HgS, the band gap was 1.82 eV, indicating a transition from semi-metallic to semiconductor behaviour of bulk  $\beta$ -HgS (0.5 eV).<sup>26</sup> The band gaps of the prepared metal sulphide nanoparticles were seen to be increased with respect to the bulk, indicating size quantization effects. The photoluminescence

spectra of the prepared nanometal sulphides were recorded at an excitation wavelength of 250 nm for HgS, as can be seen in Fig.-6. In general, the PL properties of semiconductor nanocrystals are influenced by the size of particles, crystallinity, and imperfection.<sup>27</sup> Typically, two emission peaks are observed for semiconductor nanocrystals, which can be thought to be due to sharp interstitial emission and broad trapped surface state emission, respectively.<sup>28,29</sup> The samples' broad and asymmetric emission could be attributed to size heterogeneity absence of a capping agent.<sup>30</sup>

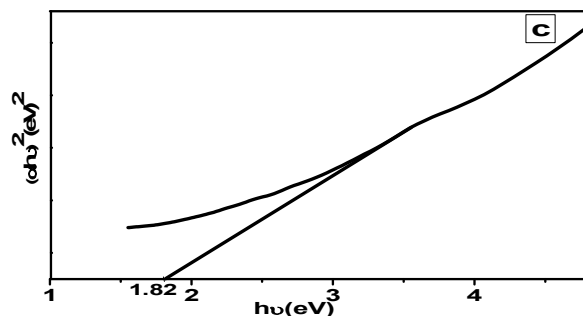


Fig.-5: Tauc Plot for HgS

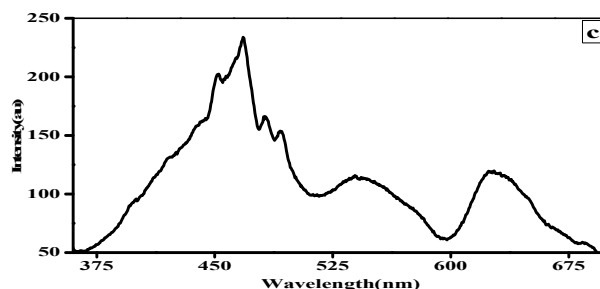


Fig.-6: PL Spectrum of HgS

The emissions in the PL phenomenon are due to different vacancies and defects related to surface states and deep-level states and could play a major role and subsequently change the nature of the emission spectra.<sup>31</sup> Variation of the surface charge density and neighbourhood fields resulted in a uniform widening of the excitonic maxima.<sup>32</sup> The broad unsymmetrical emission more toward higher wavelengths revealed the surface's influence. Here, for the HgS nanoparticles, a multi-peak emission was observed. There is a main sharp peak with high intensity observed at 468 nm with different shoulders, following which there are large emission bands at higher wavelengths mainly centred at ~539 nm and 624 nm. Sharp excitonic emission brought on by band-to-band coupling as well as a wider emission brought on by surface state or flaws at a longer wavelength.<sup>33</sup> The particle size can be determined using the Debye Scherrer formula from XRD.<sup>34</sup> Figure-7 depicts the XRD patterns of the prepared HgS nanomaterials, with diffraction intensities recorded in  $2\theta$  angles.

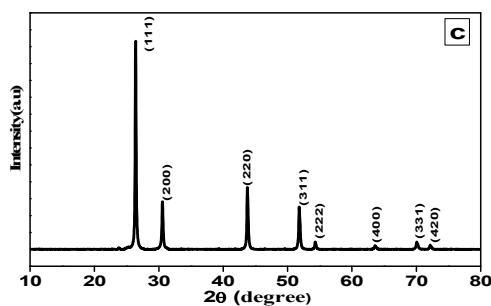


Fig.-7: XRD pattern of HgS

It shows primary diffraction patterns indexed at the planes (111), (200), (220), and (311), which confirm the planes of cubic HgS structures. The JCPDS No. (00-006-0261) card's regular patterns and the XRD patterns fit quite well. The size of HgS nanocrystals was calculated to be 43.3 nm using the Debye Scherrer equation. The lattice parameters obtained as  $5.848 \text{ \AA}$  for a, b and c are very near to the standard values  $a = b = c = 5.852 \text{ \AA}$  reported in the JCPDS file No. (00-006-0261). Also, the crystallinity percentage of the HgS nanoparticles was calculated as 95.81. As the size of the particles are not too small and is highly crystalline, the diffraction peaks for HgS are sharper. Figure-8 shows FESEM images of the synthesized HgS samples. It shows the presence of differently shaped particles, most of them are cubic and oval with uniform distribution and are seen to be highly crystalline.

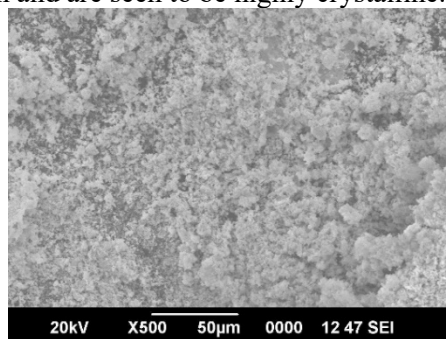


Fig.-8: SEM Images of HgS

Figure-9 illustrates how the EDX spectrum was used to assess the elementary composition and stoichiometry of produced metal sulphide nanoparticles. This shows that all the samples were pure, with the metal and S being the only elementary components.

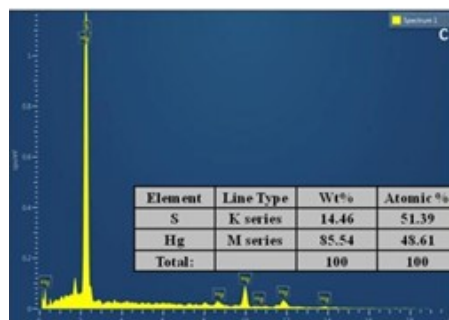


Fig.-9: EDX Spectra for HgS

For HgS Hg: S was found to be of ratio 49: 51. From the result, it is clear that they are having full compliance with the stoichiometric ratio of 1: 1. TEM of HgS nanoparticles are shown in Fig.-10.

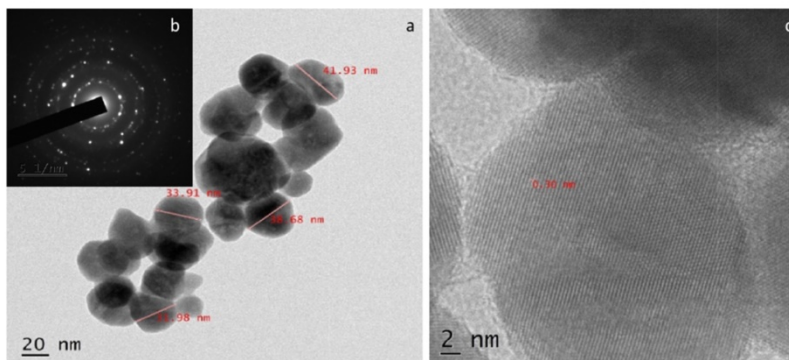


Fig.-10: TEM Images of HgS

TEM of HgS (10a) shows that the particles are highly crystalline with oval and nearly cubic shape, with size distribution from 31.98 nm to 41.93 nm with an average particle size of 36.62 nm.<sup>35</sup> The Selected Area Electron Diffraction pattern (10b) for mercuric sulphide has diffuse rings with an intense spotty

pattern in a symmetric manner indicating a cubic crystalline phase. These intense spotty patterns are due to the greater size of HgS nanocrystals compared to ZnS and CdS nanoparticles. The d spacing data obtained from the Selected Area Electron Diffraction pattern agree with the d spacing calculated from the cubic crystalline phase of HgS crystal data. The HRTEM of HgS in (10c) shows distinct crystalline nanoparticles having 0.30 nm spacing between lattices, suggesting crystal development along the (200) plane.

### CONCLUSION

The compound CDDTSC was successfully synthesized in excellent yields and was evaluated using spectroscopic techniques. Hg(II) complexes of this ligand have also been synthesized successfully. They were characterized by IR and thermal analysis before being heated up with glycerol to undergo thermal degradation. The corresponding metal sulphide nanoparticles were produced in a relatively high yield and in a well-defined, highly crystalline, and monodispersed form. The work also involved characterizing these nanoparticles. The study shows that the prepared metal complexes of the ligand CDDTSC could effectively be used as SSMPs in the nano synthesis of mercuric sulphide nanoparticles.

### ACKNOWLEDGMENT

This work was done as a part of a Ph.D. thesis at University College, Trivandrum, Kerala, and the SAIF (CUSAT) authorities provided technical support for the project, for which the authors are grateful.

### REFERENCES

1. R. Mahtab, J. P. Rogers, C. J. Murphy, *Journal of the American Chemical Society*, **117**, 9099(1995), <https://doi.org/10.1021/ja00140a040>
2. F. E. Kruis, H. Fissan, A. Peled, *Journal of Aerosol Science*, **29**, 511(1998), [https://doi.org/10.1016/S0021-8502\(97\)10032-5](https://doi.org/10.1016/S0021-8502(97)10032-5)
3. K. Sivaram, M. C. Rao, G. Giridhar, M. Tejaswi, B. T. P. Madhav, V. G. K. M. Pisipati, R. K. N. R. Manepalli, *Rasayan Journal of Chemistry*, **10**, 16(2017), <https://doi.org/10.7324/RJC.2017.1011539>
4. J. G. Brennan, T. Siegrist, P. J. Carroll, S. M. Stuczynski, L. E. Brus, M. L. Steigerwald, *Journal of the American Chemical Society*, **111**, 4141(1989), <https://doi.org/10.1021/ja00193a079>
5. M. Tejaswi, M. C. Rao, R. K. N. R. Manepalli, B. T. P. Madhav, P. Pardhasaradhi, G. Giridhar, K. Pandian, V. G. K. M. Pisipati, *Rasayan Journal of Chemistry*, **10**, 69(2017), <https://doi.org/10.7324/RJC.2017.1011571>
6. P. S. Nair, T. Radhakrishnan, N. Revaprasadu, G. Kolawole, P. O'Brien, *Journal of Materials Chemistry*, **12**, 2722(2002), <https://doi.org/10.1039/b202072f>
7. C. T. Handoko, A. Huda, M. D. Bustan, B. Yudono, F. Gulo, *Rasayan Journal of Chemistry*, **10**, 1137(2017), <https://doi.org/10.7324/RJC.2017.1041875>
8. J. George, G. R. Nath, V. S. Lekha, K. Rajesh, *Asian Journal of Chemistry*, **34**, 2055(2022), <https://doi.org/10.14233/AJCHEM.2022.23742>
9. P. Vijaya Kumar, S. Mary Jelastin Kala, K. S. Prakash, *Rasayan Journal of Chemistry*, **11**, 1544(2018), <https://doi.org/10.31788/RJC.2018.1144044>
10. R. K. Agarwal, L. Singh, D. K. Sharma, *Bioinorganic Chemistry and Applications*, **2006**, 1(2006), <https://doi.org/10.1155/BCA/2006/59509>
11. A. Umar, S. A. Andrani, S. M. Choi, Y. K. Krisnandi, *Rasayan Journal of Chemistry*, **12**, 1613(2019), <https://doi.org/10.31788/RJC.2019.1235244>
12. P. Rapheal, E. Manoj, *Polyhedron*, **26**, 5088(2007).
13. D. Kovala-Demertzi, A. Papageorgiou, L. Papathanasis, A. Alexandratos, P. Dalezis, J. R. Miller, M. A. Demertzis, *European Journal of Medicinal Chemistry*, **44**, 1296(2009), <https://doi.org/10.1016/j.ejmech.2008.08.007>
14. R. Manikandan, P. Vijayan, P. Anitha, G. Prakash, P. Viswanathamurthi, R. J. Butcher, K. Velmurugan, R. Nandhakumar, *Inorganica Chimica Acta*, **421**, 80(2014), <https://doi.org/10.1016/j.ica.2014.05.035>
15. M. Joseph, V. Suni, M. R. Prathapachandra Kurup, M. Nethaji, A. Kishore, S. G. Bhat, *Polyhedron*, **23**, 3069(2004), <https://doi.org/10.1016/j.poly.2004.09.026>
16. S. Chandra, Y. Kumar, *Proceedings of the Indian Academy of Sciences-Chemical Sciences*, **92**, 2809

- 249(1983), <https://doi.org/10.1007/BF02841242>
17. A. S. Reddy, L. S. Krishna, H. K. Rashmi, P. U. M. Devi, Y. Sarala, A. V. Reddy, *Journal of Applied Pharmaceutical Science*, **6**, 107(2016), <https://doi.org/10.7324/JAPS.2016.601015>
  18. M. J. M. Campbell, R. Grzeskowiak, R. Thomas, M. Goldstein, *Spectrochimica Acta Part A: Molecular Spectroscopy*, **32**, 553(1976), [https://doi.org/10.1016/0584-8539\(76\)80116-X](https://doi.org/10.1016/0584-8539(76)80116-X)
  19. S. Chandra, M. Tyagi, *Journal of the Serbian Chemical Society*, **73**, 727(2008), <https://doi.org/10.2298/JSC0807727C>
  20. V. B. Rana, P. C. Jain, M. P. Swami, A. K. Srivastava, *Journal of Inorganic and Nuclear Chemistry*, **37**, 1826(1975), [https://doi.org/10.1016/0022-1902\(75\)80336-8](https://doi.org/10.1016/0022-1902(75)80336-8)
  21. R. K. Agarwal, L. Singh, D. K. Sharma, *Bioinorganic Chemistry and Applications*, **2006**, (2006), <https://doi.org/10.1155/BCA/2006/59509>
  22. T. Xaba, B. Masinga, *Journal of Nanomaterials*, **11**, 1231(2016).
  23. G. Pandey, H. K. Sharma, *Synthesis and Reactivity in Inorganic, Metal-Organic and Nano-Metal Chemistry*, **40**, 312(2010), <https://doi.org/10.1080/15533174.2010.486816>
  24. S. N. Shukla, P. Gaur, N. Rai, *Applied Nanoscience*, **5**, 583(2015), <https://doi.org/10.1007/s13204-014-0351-0>
  25. B. Srinivasa Rao, B. Rajesh Kumar, G. Venkata Chalapathi, V. Rajagopal Reddy, T. Subba Rao, *Journal of Nano- and Electronic Physics*, **3**, 620(2011).
  26. S. Rath, S. N. Sarangi, S. N. Sahu, *Applied Physics A: Materials Science and Processing*, **86**, 447(2007), <https://doi.org/10.1007/s00339-006-3812-9>
  27. D. C. Onwudiwe, T. P. J. Krüger, C. A. Strydom, *Materials Letters*, **116**, 154(2014), <https://doi.org/10.1016/j.matlet.2013.10.118>
  28. B. Geng, J. Ma, F. Zhan, *Materials Chemistry and Physics*, **113**, 534(2009), <https://doi.org/10.1016/j.matchemphys.2008.08.006>
  29. M. O'Neil, J. Marohn, G. McLendon, *Journal of Physical Chemistry*, **94**, 4356(1990), <https://doi.org/10.1021/j100373a089>
  30. G. Murugadoss, *Particuology*, **10**, 722(2013)
  31. K. S. Prasad, T. Amin, S. Katuva, M. Kumari, K. Selvaraj, *Arabian Journal of Chemistry*, **10**, S3929(2017), <https://doi.org/10.1016/J.ARABJC.2014.05.033>
  32. S. Kar, S. Panda, S. Satpati, B. Satyam, P. V. Chaudhuri, *Nanoscience Nanotechnology*, **6**, 771(2006), <https://doi.org/10.1166/jnn.2006.078>
  33. Dezhi, Y. Guangrui, Z. Li, D. Xian, W. Yabo, Qin, *Bulletin of the Korean Chemical Society*, **35**, 1077(2014), <https://doi.org/10.5012/bkcs.2014.35.4.1077>
  34. C. F. Holder, R. E. Schaak, *ACS Nano*, **13**, 7359(2019), <https://doi.org/10.1021/ACS.NANO.9B05157>
  35. J. Hambrock, A. Birkner, R. F. Chemistry, *Journal of Materials Chemistry*, **11**, 3197(2001).

[RJC-6928/2021]